

# ON THE MICROSCOPIC NATURE OF THE PHOTON STRENGTH FUNCTION

Achakovskiy O.I.<sup>1</sup>, Avdeenkov A.V.<sup>1</sup>, Kamerdzhev S.P.<sup>2</sup>

<sup>1</sup> Institute for Physics and Power Engineering, Obninsk, Russia

<sup>2</sup> Institute for Nuclear Power Engineering NRNU MEPHI, Obninsk, Russia

The E1 photon strength functions (PSF) of several Ni and Sn even-even isotopes have been calculated microscopically within the self-consistent version of the Extended Theory of Finite Fermi Systems which includes the QRPA approach and, in addition, phonon coupling. The calculations are fully self-consistent in the sense that the HFB mean field, effective interaction and phonons have been calculated using the Skyrme force Sly4 with the known parameters. On the contrary to the usual phenomenological approaches, these PSFs have structures, the most interesting ones being in the energy region of the pygmy-dipole resonance. These structures are caused both by the QRPA and the phonon coupling effects. The microscopically obtained PSFs have been used in the EMPIRE3.1 code to calculate characteristics of nuclear reactions, namely, radiative capture cross sections for  $^{115}\text{Sn}(n,\gamma)$  and  $^{119}\text{Sn}(n,\gamma)$  and, for the first time, average radiative widths. In all considered properties, the contribution of phonon coupling turned out significant. A reasonable agreement with the available experimental data has been obtained, including the explanation of the PSF in the pygmy-dipole resonance energy region for  $^{116}\text{Sn}$  and radiative capture cross sections for  $^{115}\text{Sn}(n,\gamma)$  and  $^{119}\text{Sn}(n,\gamma)$ .

## INTRODUCTION

The information about photon strength function (PSF) is necessary to calculate all characteristics of nuclear reactions with gamma-rays, in particular, the radiative neutron capture cross sections, which are of great astrophysical [1] and nuclear engineering [2] interest. The usual definition of PSF contains transitions between excited states. In order to calculate PSFs, as a rule, the known Brink-Axel hypothesis is used, which states that on each excited state it is possible to build a giant dipole resonance (at present, any giant resonance) *including its low-lying part*. Thus, the PSF is a rather complicated notion and includes at least two questions, namely, the validity of this hypothesis (that is considered at present as reasonable) and what kind of resonance is excited in the de-excitation process. In this article, we will try to answer the latter question.

In the low-lying part of giant dipole resonance, in the energy region between zero and near the nucleon separation energy, to be exact, there exists the so-called Pygmy-Dipole Resonance (PDR). It typically exhausts about (1-2)% of the Energy Weighted Sum Rule (EWSR) but, nevertheless, it can significantly increase the radiative neutron capture cross section and affect the nucleosynthesis of neutron-rich nuclei by the r-process [1]. However, it turned out that in neutron-rich nuclei, for example,  $^{68}\text{Ni}$  [3] and, probably,  $^{72}\text{Ni}$ ,  $^{74}\text{Ni}$ , this fraction is much larger. It is also necessary to note that for nuclei with small neutron separation energy, less than 3-4 MeV, the PDR properties are changed significantly [1], and therefore, phenomenological systematics obtained by fitting characteristics of stable nuclei (with separation energy of about 8 MeV) is not suitable. If the Brink-Axel hypothesis is valid, the PSF is connected very simply with the photoabsorption cross section [4, 5] and therefore, with the PDR field [5, 6, 7].

For all these reasons, during the last decade there was an increasing interest in the investigations of the excitations in the PDR energy region manifested both in “pure” low-energy nuclear physics [6, 7] and in the nuclear data field [1, 4, 8].

As a rule, in the nuclear data field only phenomenological models for PDR and PSF, based on various improvements of the Lorentzian-type approximation, are used, see the dashed region in Fig.1. There six phenomenological PSF models taken from RIPL [4, 8] are shown. However, as it was noted in RIPL2 [4] and RIPL3 [8], the phenomenological Lorentzian-based expressions for PSF suffer from various shortcomings: in particular, “they are unable to predict the resonance-like enhancement of the E1 strength at energies below the neutron separation energy” and “this approach lacks reliability when dealing with exotic nuclei”. For these reasons, since 2006 the microscopic self-consistent PSFs calculated within the Hartree-Fock-Bogolyubov method and Quasiparticle Random Phase Approximation (HFB+QRPA) [1] have been included in RIPL2 [4], RIPL3 [8] and in modern nuclear reaction codes, like EMPIRE [9] and TALYS [10]. Such an approach is very natural because it uses the single-particle properties of each nucleus and is of higher predictive power in comparison with phenomenological models. However, as discussed below and confirmed by modern experiments, the HFB+QRPA approach is necessary but not sufficient. To be exact, it should be complemented by the effect describing the interaction of single-particle degrees of freedom with the low-lying collective phonon degrees of freedom, or phonon coupling (PC).

Recent experiments in the PDR energy region [11, 12, 13] have given additional information about the PDR and PSF. The PSF structures at 8-9 MeV in six Sn isotopes obtained by the Oslo method [12] could not be explained within both the standard phenomenological approach [12] and the microscopic HFB+QRPA approach [13]. In both cases, to explain the experiment, it was necessary to add “by hand” some additional strength of about 1-2 % of the EWSR. The results [13] directly confirm the necessity to improve the HFB+QRPA method. In particular, the PC effects discussed in [14, 16] may be a source of such extra strength.

In this work, we use the self-consistent version of the extended theory of finite Fermi systems (ETFFS) [14] in the quasi-particle time blocking approximation (QTBA) [15].

Our ETFFS (QTBA) method, hereinafter as QTBA, includes self-consistently the QRPA and PC effects and the single-particle continuum in a discrete form. We calculate the microscopic PSFs in several Sn and Ni isotopes and use them in the EMPIRE codes to estimate the neutron radiative capture cross sections and average radiative widths.

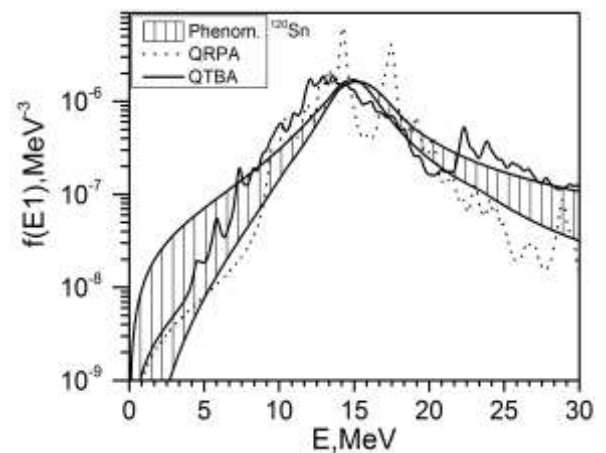


**Fig. 1.** PSF for  $^{120}\text{Sn}$  as a function of energy  $E$ . The dashed region is an estimate of the systematic uncertainties of six phenomenological models from the RIPL2 database [4]. Dotted line: self-consistent QRPA. Full line: QTBA (final results with PC)

## PHOTON STRENGTH FUNCTIONS. INTEGRAL CHARACTERISTICS OF PDR AND GDR

To calculate the standard strength function  $S(\omega)=dB(E1)/dE$  and, therefore, PSF, we use the well-known Sly4 Skyrme force [17]. The ground state is calculated within the HFB method using the spherical code HFBRAD [18]. The residual interaction for the QRPA and QTBA calculations is derived as the second derivation of the Skyrme functional. In all our calculations, we use the smoothing parameter of 200keV.

In Fig.1, six phenomenological Lorentzian-type models of the E1 PSF [4] for  $^{120}\text{Sn}$  are shown together with our QRPA and QTBA results (QTBA being QRPA+PS). In Fig.2, Fig.3 and Fig.4, we show the PSFs

in the PDR and GDR energy regions together with the available experimental data of the Oslo method for the  $^{116}\text{Sn}$  PDR energies. We have found the following:

1) In contrast to phenomenological models (Fig.1), in all the nuclei under consideration, there are structures caused by both QRPA and PC effects, the latter ones being just in the 8-9 MeV region observed in Sn isotopes [12].

2) for the PSF for  $^{116}\text{Sn}$  in the PDR region we obtained a good agreement with the experiment [12] which can be explained only by the PC contribution, especially at  $E>4$  MeV. Probably, the main reason of such a successful description is the fact that our smoothing parameter approximately coincides with the experimental resolution in [12].

3) As it should be expected, the EGLO description has no structures.

Comparing with the GDR energy region results in Fig.2 and Fig.3, one can see “by sight”

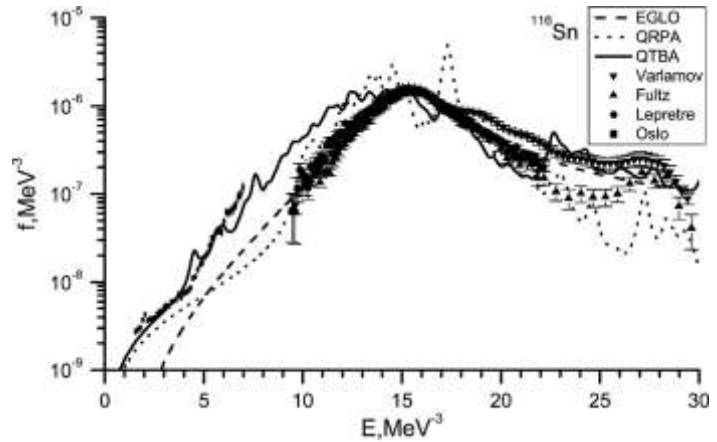


**Fig. 2.** The E1 PSF for  $^{116}\text{Sn}$  in the PDR and GDR energy region. Dotted line: self-consistent QRPA. Full line: QTBA (final results with PC). Dashed line: Enhanced Generalized Lorentzian (EGLO) model [4]. Experimental data are taken from [22, 20, 21, 12].

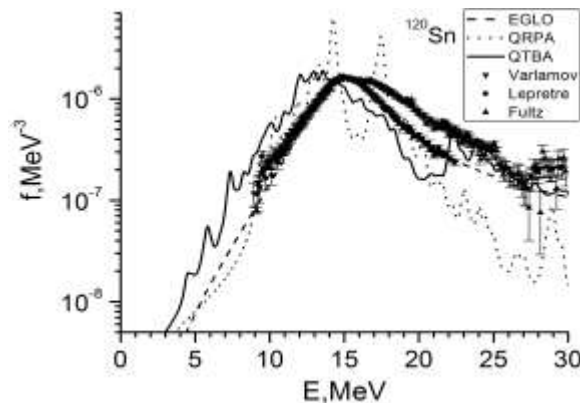


**Fig. 3.** The E1 PSF for  $^{120}\text{Sn}$  in the PDR and GDR energy region. Dotted line: self-consistent QRPA. Full line: QTBA (final results with PC). Dashed line: Enhanced Generalized Lorentzian (EGLO) model [4]. Experimental data are taken from [22, 21, 20].

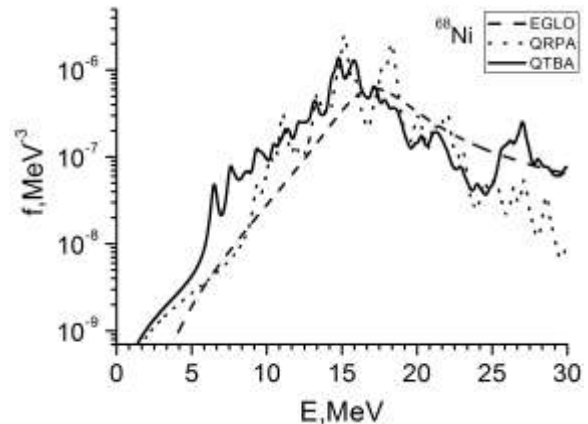


**Fig. 4.** E1 PSF for  $^{68}\text{Ni}$ . Dotted line: self-consistent QRPA. Full line: QTBA (final results with PC). Dashed line: Enhanced Generalized Lorentzian (EGLO) model [4].

that there is some disagreement with the experiment in this region. So we have made calculations of the integral characteristics in the ( $S_n$ -30) MeV interval, which is a typical interval for the GDR measurements. The calculations have been performed with the use of the standard moment method [14, 16]:

$$\langle E \rangle = E_{1,0} = \frac{m_1}{m_0}, \quad D = \sqrt{\frac{m_2}{m_0} - \left(\frac{m_1}{m_0}\right)^2}, \quad (1)$$

where the energy moments  $m_k$  for energy interval  $\Delta E = E_{max} - E_{min}$  are calculated as follows

$$m_k = \int_{E_{min}}^{E_{max}} S(E) E^k dE. \quad (2)$$

The results are given in Table 1. One can see that, on the whole, we obtained a reasonable agreement with experiment. Note that in our calculations of the standard strength function the velocity terms of the Skyrme interaction were considered, see [16], so we obtained about 125% for the EWSR percent exhausted in Sn isotopes. A difference of the QTBA values from the experimental EWSR data are caused by the fact that for this case it is necessary to integrate up to 35MeV, and for this ( $S_n$ -35) MeV interval the QTBA EWSR results almost coincide with the QRPA ones which have been obtained for both intervals. Also, in Table 1 the experimental errors are shown (in brackets), they were obtained by us from the experimental errors presented in the experimental articles.

Table 1. Integral characteristics of the E1 excitations in the ( $S_n$ -30) MeV interval, see text for details.									
		$^{116}\text{Sn}$	$^{118}\text{Sn}$	$^{120}\text{Sn}$	$^{124}\text{Sn}$	$^{58}\text{Ni}$	$^{62}\text{Ni}$	$^{68}\text{Ni}$	
$\langle E \rangle, \text{MeV}$	EGLO	17.00	16.88	16.82	16.71	19.51	19.16	18.73	
	QRPA	15.74	15.61	15.36	15.23	19.01	17.97	16.82	
	QTBA	16.21	16.09	15.82	15.57	18.92	17.98	16.86	
	exp.	[20]							[24]
		16.85 (15)	17.76 (18)	17.57 (17)	17.01 (24)				18.1(5)
	[22]					[23]			
	17.57 (14)	17.32 (16)	17.37 (14)	17.10 (6)	20.43				
$D, \text{MeV}$	EGLO	4.07	4.05	4.11	4.10	3.81	3.97	4.06	
	QRPA	3.07	3.12	3.07	3.10	3.54	3.36	3.16	
	QTBA	4.55	4.63	4.61	4.45	4.14	4.49	4.42	
	exp.	[20]							[24]
		3.78 (15)	4.30 (15)	4.27 (10)	4.17 (21)				6.1 (5)
	[22]					[23]			
	4.17 (12)	4.28 (15)	4.29 (13)	4.13 (20)	3.98				
% EWSR	EGLO	114.3	112.9	118.0	107.5	93.7	96.3	98.8	
	QRPA	136.1	135.1	132.3	134.0	140.2	129.8	123.0	
	QTBA	125.5	124.9	124.6	127.3	122.9	112.2	113.3	
	Exp.	[20]							
		97.9 (70)	139.6 (71)	158.3 (73)	154 (11)				
	[22]					[23]			
	137.1 (79)	148.4 (85)	157.7 (83)	144 (10)	96.8				

Recently, the PDR characteristics in the unstable neutron-rich  $^{68}\text{Ni}$  nucleus have been measured [3] and rather expressive results have been obtained: the PDR in this nucleus exists in the (7-13) MeV interval, with the mean energy of about 11 MeV and about 5 percent of EWSR exhausted (the latter might be between 5 and 9 % [19]). Note that the neutron separation energy of  $^{68}\text{Ni}$  is 7.8 MeV, i.e. the PDR is much higher than the separation energy.

Using the moments method for this energy interval (without a Lorentzian approximation), we obtained a reasonable agreement with the experiment [3]. Namely, we found the PDR with the mean energy of 10.9 MeV and 10.2 % of EWSR exhausted for the QTBA model and, correspondingly, 11.2 MeV and 6.4 % for the QRPA model. Earlier, the similar calculations had been performed within the relativistic QTBA [19], with two phonon contributions additionally taken into account. In other words, the authors [19] were forced to change their model in order to explain the experiment.

### RADIATIVE NEUTRON CAPTURE

It is of great interest to investigate the PC contribution to characteristics of radiative nuclear reactions. In Fig. 5, the radiative neutron capture cross sections for  $^{115}\text{Sn}(n,\gamma)$  and  $^{119}\text{Sn}(n,\gamma)$  calculated with the use of our self-consistent QRPA and QTBA models are presented. The EMPIRE3.1 code with the GSM model for nuclear level density has been used. For both reactions, a reasonable agreement with the experiment has been obtained only due to the fact that PC was taken into account. In addition, it should be pointed out that no fitting was used in our QTBA approach. The agreement with the EGLO model is reasonable because the parameters of PDR and GDR were fitted for these stable nuclei, see [4, 8].

The results of our calculations of the corresponding capture gamma-ray spectra are presented in the poster paper [29] at this Seminar.

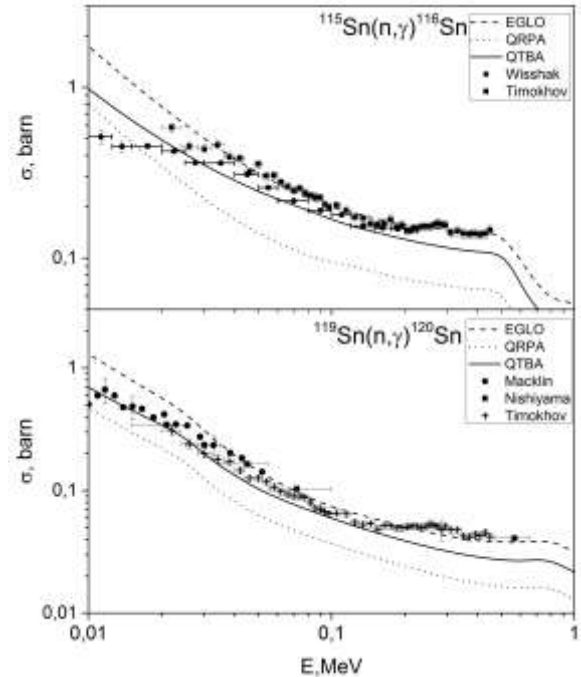


**Fig. 5.** Radiative capture cross sections for  $^{115}\text{Sn}(n,\gamma)^{116}\text{Sn}$  and  $^{119}\text{Sn}(n,\gamma)^{120}\text{Sn}$ .

Experimental cross sections are taken from Refs. [25–28]

### AVERAGE RADIATIVE WIDTHS

Average radiative widths of neutron resonances  $\Gamma_\gamma$  are very important characteristics of gamma-decay for which there are a lot of experimental data [2]. We have calculated the widely used quantity  $2\pi\Gamma_\gamma/D_0$  with the EGLO and our QRPA and QTBA PSF models and the GSM nuclear level density model [4] for the s-wave spacing  $D_0$  (Table 2). As far as we know, these are the first calculations of  $\Gamma_\gamma$  performed with PC. We have found that, except for  $^{68}\text{Ni}$ , the PC increases the QRPA contribution by 100-200% in the direction to the systematics [30]. Note that the comparison with the experiment in  $^{118}\text{Sn}$ ,  $^{120}\text{Sn}$  and  $^{62}\text{Ni}$  may give some information about the contribution of M1 resonance.

Table 2. Quantities $2\pi\Gamma_\gamma/D_0$ for s-neutrons where $\Gamma_\gamma$ is the average radiative width (see text for details). The experimental data (underlined) and systematics are taken from [2] and [30], respectively.				
Nuclei	EGLO	QRPA	QTBA	<u>Exp. or systematics</u>
$^{116}\text{Sn}$	$7.99*10^{-3}$	$3.33*10^{-3}$	$5.14*10^{-3}$	$11.73*10^{-3}$
$^{118}\text{Sn}$	$7.94*10^{-3}$	$3.77*10^{-3}$	$5.64*10^{-3}$	<u><math>8.24*10^{-3}</math></u>
$^{120}\text{Sn}$	$5.77*10^{-3}$	$2.49*10^{-3}$	$3.58*10^{-3}$	<u><math>6.98*10^{-3}</math></u>
$^{124}\text{Sn}$	$4.77*10^{-3}$	$2.13*10^{-3}$	$2.67*10^{-3}$	$9.84*10^{-3}$
$^{58}\text{Ni}$	$7.04*10^{-3}$	$2.30*10^{-3}$	$7.33*10^{-3}$	$17.0*10^{-3}$
$^{62}\text{Ni}$	$2.51*10^{-3}$	$1.97*10^{-3}$	$4.33*10^{-3}$	<u><math>5.98*10^{-3}</math></u>
$^{68}\text{Ni}$	$1.04*10^{-4}$	$4.73*10^{-5}$	$2.46*10^{-4}$	$2.64*10^{-4}$

## CONCLUSION

We have shown that our microscopic ETFFS(QTBA) approach gives structures for PSF caused by both the QRPA and PC effects, the latter being in the observed 8-9 MeV region for Sn isotopes. The integral characteristics of the PDR in  $^{68}\text{Ni}$  have been explained within this approach. The observed PSF in the PDR region for  $^{116}\text{Sn}$  can be explained only by the PC effects, especially at  $E > 4$  MeV. Except for the  $^{68}\text{Ni}$  case, the PC contribution increases the average radiation widths by 100-200% in the direction to the systematics, which indirectly confirms the necessity of taking PC into account. The results for average radiative strength in  $^{118}\text{Sn}$ ,  $^{120}\text{Sn}$  and  $^{62}\text{Ni}$  are especially interesting because the comparison with the available experimental data makes it possible to obtain some information about the contribution of M1 resonance to these properties (it will be made somewhere else). The last but not the least, the neutron radiative capture cross sections for  $^{115}\text{Sn}(n,\gamma)$  and  $^{119}\text{Sn}(n,\gamma)$  could be explained by the inclusion of the PC effects. Thus, the results obtained clearly show the necessity of taking the PC effects into account in the microscopic theory of radiative nuclear data. The self-consistent method used is of particular relevance for nuclear astrophysics. We will apply our method to many other stable and unstable nuclei, in particular, for the prediction of the PDR characteristics in the neutron-rich  $^{72}\text{Ni}$  and  $^{74}\text{Ni}$ .

The authors express their appreciation to the ISINN22 Organizing Committee for the support.

S.K. acknowledges Drs. A. Sukhovej and V. Furman for useful discussions.

## Bibliography

1. S. Goriely, E. Khan, V. Samyn, Nucl. Phys. A **739**, 331 (2004).
2. S.F. Mughabghab, *Atlas of neutron Resonances, Resonance Parameters and Thermal Cross Sections Z=1-100* (Elsevier, Amsterdam, 2006).
3. O. Wieland, *et al.*, Phys. Rev. Lett. **102**, 092502 (2009).
4. *Reference Input Parameter Library, RIPL-2*, IAEA-TECDOC-1506, 2006. See also <https://www-nds.iaea.org/RIPL-2> (2006).
5. S.P. Kamerdzhiev, A.V. Avdeenkov, O.I. Achakovskiy, Phys. Atom. Nucl. **77**, 1303 (2014).

6. D. Savran, T. Aumann, A. Zilges, *Prog. Part. Nucl. Phys.* **70**, 210 (2013).
7. N. Paar, D. Vretenar, E. Khan, G. Colo, *Rep. Prog. Phys.* **70**, 691 (2007).
8. R. Capote *et al.*, *Nuclear Data Sheets* **110**, 3107 (2009). See also <https://www-nds.iaea.org/RIPL-3>.
9. R. Herman, R. Capote, B.V. Carlson, P. Oblozinsky, M. Sin, A. Trkov, H. Wienke, V. Zerkin, *Nucl. Data Sheets*, **108** 2655 (2007).
10. A.J. Koning and D. Rochman, *Nuclear Data Sheets* **113**, 2841 (2012).
11. R. Schwengner *et al.*, *Phys. Rev. C* **87**, 024306 (2013).
12. H.K. Toft, *et al.*, *Phys. Rev. C* **83**, 044320 (2011).
13. H. Utsunomiya, *et al.*, *Phys. Rev. C* **84**, 055805 (2011).
14. S. Kamezdzhiev, J. Speth, G. Tertychny, *Phys. Rep.* **393**, 1 (2004).
15. V. Tselyaev, *Phys. Rev. C* **75**, 024306 (2007).
16. A. Avdeenkov, S. Goriely, S. Kamezdzhiev, S. Krewald, *Phys. Rev. C* **83**, 064316 (2011).
17. E. Chabanat, P. Bonche, P. Haensel, *Nucl. Phys. A* **635**, 231 (1998).
18. K. Bennaceur and J. Dobaczewski, *Comp. Phys. Comm.* **168**, 96 (2005).
19. E. Litvinova, P. Ring, V. Tselyaev, *Phys. Rev. Lett.* **105**, 022502 (2010).
20. S.C. Fultz *et al.*, *Phys. Rev.*, **186**, 1255 (1969).
21. A. Lepretre, *et al.*, *Nucl. Phys. A* **219**, 39 (1974).
22. V.V. Varlamov, *et al.*, *Moscow State Univ. Inst. of Nucl. Phys. Reports*, No.2009, p.3/847 (2009).
23. V. V. Varlamov, *et al.*, *Izv. Ros. Akad. Nauk, Ser. Fiz.* **67**, 656(2003).
24. D. Rossi, P. Adrich, F. Aksouth, *et al.*, *J. Phys. Conf. Ser.* **420**, 012072 (2013).
25. K. Wisshak, *et al.*, *Phys. Rev. C* **54**, 1451 (1996).
26. V.M. Timokhov, *et al.*, *Fiz.-Energ. Institut, Obninsk Reports* No.1921 (1988).
27. R.L. Macklin, T. Inada, J.H. Gibbons, *Washington AEC Office Reports*, No.1041, p.30 (1962).
28. J. Nishiyama, M. Igashira, T. Ohsaki, *et al.*, *J. Nucl. Sci. Technol. (Tokyo)* **45**, 352 (2008).
29. O.I. Achakovskiy, A.V. Avdeenkov, S.P. Kamezdzhiev, D.A. Voitenkov, this Seminar
30. *Reference Input Parameter Library, RIPL-1*, IAEA-TECDOC-1034 (1998).